Global NEST Journal, Vol 27, No 4, 06782

Interaction and quantum chemical analysis between sulfamethoxazole and copper on biochar

Zhong J.[1, 2*], He J.[1], Bao Y.[3], Zhang Y.[1], Gao Y.[1], Li J.[1] and Liu L.[1]
[1]School of Environmental and Municipal Engineering, Lanzhou Jiaotong University, Lanzhou, 730070, China
[2]Key laboratory of Yellow River Water Environment in Gansu Province, Lanzhou, 730070, China
[3]State Key Laboratory of Water Resource Protection and Utilization in Coal Mining, National Institute of Clean and Low Carbon Energy, Beijing 102209, China
Received: 06/09/2024, Accepted: 28/01/2025, Available online: 10/02/2025
*to whom all correspondence should be addressed: e-mail: zhongjk@mail.lzjtu.cn
https://doi.org/10.30955/gnj.06782

Graphical abstract

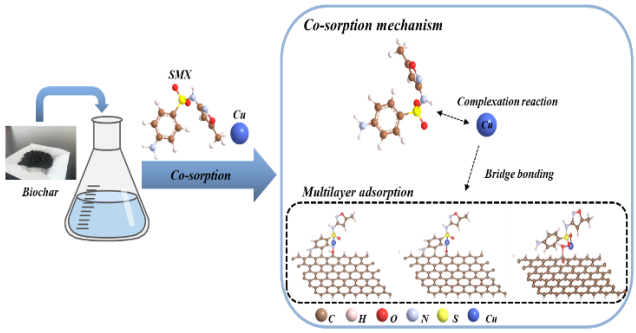

Abstract

Sulfamethoxazole (SMX) and copper (Cu) are common antibiotic and heavy metallic contaminants. They can be removed separately through biochar sorption method. However, the interaction between SMX and Cu remains an unresolved issue in the sorption process of biochar. In this paper, two biochar samples were prepared from maize straw at temperatures of 300 °C and 600 °C. The interaction between SMX and Cu in the sorption process on biochar was investigated using the batch equilibrium experiment method and quantum chemical calculations. The results showed that co-existing of SMX and Cu has a significant contribution to each other's sorption on biochar. In the coexisting system of SMX and Cu, the sorption capacity of HBC600 for SMX and Cu were 24.22 mg/g and 96.23 mg/g, which were higher than the single system. Quantum chemical calculations showed that due to the bridge bonding and complexation of Cu and SMX on the biochar, the biochar may have formed OH-Cu-SMX, CO-Cu-SMX and COOH-Cu-SMX bonds with the pollutants in the mixed system, and the sorption energy was significantly increased. This indicates that the sorption capacity of biochar for both pollutants was enhanced in the mixed system.

Keywords: biochar, co-sorption, interaction, quantum chemical calculation

1. Introduction

The combined pollution from antibiotics and heavy metals (HMs) is attracting widespread attention in recent years (Yao *et al.*2020; Zhao *et al.*2022). Sulfamethoxazole (SMX), a typical sulfonamide antibiotic, which has been frequently observed in the surface water, groundwater and soil(Gao *et al.*2014), is difficult to remove using classic wastewater treatment methods(Younes *et al.*2019). Numerous studies have demonstrated that the antibiotic not only stimulates the emergence of drug-resistant bacteria, but also hampers the proliferation of microorganisms and plants, inflicting serious damage on the ecological environment and human health (Han *et al.*2020; Yao *et al.* 2012). Copper (Cu), a common type of heavy metals, is widely used in industry and agriculture. Due to its non-biodegradability and strong toxicity, Cu is one of the major heavy metal pollutants posing a serious threat to the ecosystem and public health(Yan *et al.*2010). The presence of antibiotics and heavy metals can be detected in many water bodies and soils, and the combined coexistence of two contaminants in the physical environment is frequently seen (Khurana *et al.*2021; Shen *et al.*2023a). Co-existing contaminants of antibiotics and HMs have joint toxic effects on organisms such as synergistic (Liu *et al.*2021), antagonistic (Tong *et al.*2015), or additive effects (You *et al.*2022), which complicate the impact on the environment (Shu *et al.*2024[cited 2024 August 16];[71 p.]). Moreover, As the interaction of functional groups on antibiotics with HMs ions (Cuprys *et al.*2018; Huang *et al.*2017; Yang *et al.*2022b), the combined contaminants are more difficult to remove than the single contaminants (Li *et al.*2018). For example, the amino functional groups and the N-heteroaromatic rings of sulfamerazine maybe interact with Cu, and tend to form complexes, weakening the reactivity of sulfamerazine molecules (Sha *et al.*2022). Therefore, it is necessary to explore the interaction mechanisms of combined contaminants of antibiotics and HMs on biochar to find an effective treatment method for them.

Last years, various techniques, such as adsorption, biodegradation, and electrochemical methods, have been developed and applied to combined pollution problems (Li *et al.*2022; Liu *et al.*2023; Long *et al.*2021). Of them, adsorption method is a low-cost, cost-effect and environmentally friendly method for pollutants removal. A variety of materials can serve as adsorbents, including carbon nanotube, alumina, activated carbon and biochar (Shan *et al.*2015). Among these materials, biochar, as an environmentally friendly material, has become a popular adsorbent for the removal of organic and inorganic pollutants from polluted water due to its high porosity, large specific surface area and rich functional groups (e.g. -COOH, -OH and C=O) that can be involved in sorption (Guo *et al.*2020). Currently, some researchers have conducted various studies to examine the effectiveness and mechanisms of biochar in the individual adsorption of HMs or antibiotics (Hu *et al.*2023; Pathy *et al.*2023; Qiu *et al.*2019; Truong *et al.*2022). However, due to the complex interaction mechanisms of combined pollutants that different antibiotic-HMs combined pollutants may exhibit either promoting or inhibiting effects on the sorption behavior of different materials (Deng *et al.*2019; Wang *et al.*2019; Yuan *et al.*2019), reports on the effect of antibiotic-HMs combined pollutants on the sorption behavior of biochar are still very limited. Therefore, in this paper, a comparative study of the sorption of single and combined systems of antibiotics and HMs was conducted to understand the sorption behavior and interaction of these contaminants coexisting in biochar. SMX and Cu were selected as representatives of antibiotics and HMs, respectively. Sorption experiments were carried out using the batch equilibrium experiment method to determine the sorption data for single and combined pollutants of SMX and Cu by biochar. Based on the experimental results, the quantum chemical calculation was performed. The formation energies of the main chemical bonds on the biochar surface were calculated by first principles using VASP (Vienna Ab mitio Simulation Package) software. The sorption mechanisms and interaction among biochar, SMX and Cu in the sorption process were explored which provides theoretical support for the feasibility of removing antibiotic-HMs combined pollutants by biochar.

2. Materials and methods

2.1. Sample preparation

Sulfamethoxazole (SMX), purchased from Chongqing Cypress Technology Co., Ltd., was prepared as a 100 mg/L stock solution with a background solution containing 0.01 mol/L $NaNO_3$ and 0.1% NaN_3. Cu $(NO_3)_2{\cdot}3H_2O$, obtained from Sinopharm Group Chemical Reagent Co., Ltd., was prepared as a 1000 mg/L stock solution with deionized water. The pH was adjusted to 5 with 0.1 mol/L HCl and 0.1 mol/L NaOH solution. All the chemicals were analytical reagents.

Maize straw, collected from a farmland in Gansu province, China, was chopped, passed through a 0.425 mm sieve, and converted to biochar by slow pyrolysis in a muffle furnace (SX2, Shanghai Jiazhan Instrument Equipment Co., Ltd.) at 300 °C or 600 °C for 6 h in a nitrogen atmosphere. The resultant biochar samples were abbreviated as BC300 and BC600. The biochar samples were then crushed and sieved to obtain uniform 0.425 mm-sized particles. The biochar samples were washed several times with 1 mol/L HCl and deionized water to remove ash until the pH value remained constant. The resulting biochar samples were labeled HBC300 and HBC600. After the biochar samples were dried at 80 °C for 12 h, they were stored in a sealed container for future use.

2.2. Characterization of the biochar

Total carbon (C), nitrogen (N), hydrogen (H), and sulfur (S) in the biochar were determined using an elemental analyzer (Vario EL, a German element company). Oxygen content was determined by mass balance (Kwak *et al.*2019). Ash content was measured by heating the biochar samples at 650 ± 20°C to a constant weight and calculated using equation (1). The yield of biochar was calculated according to equation (2). Biochar functional groups were characterized using Fourier transform infrared spectrometer (FTIR) (Nexus 870, Nicolet, USA). The specific surface area, total pore volume, and pore size distribution of the biochars were measured using the nitrogen degassing method (Alfaro Soto *et al.*2019). The micromorphology features of biochar were observed by scanning electron microscope (SEM) (JSM-5600LV, Japan Electron Optics).

$$ash = \frac{m_2 - m_1}{m} \times 100\% \quad (1)$$

where m is the mass of the original biochar sample, g; m_1 is the mass of the empty crucible after burning, g; m_2 is the mass of the crucible with biochar after ashing the original biochar at 650 °C ± 20 °C to constant weight and cooling, g.

$$yield = \frac{m_3 - m_1}{m_2 - m_1} \times 100\% \quad (2)$$

where m_1 is the mass of the crucible, g; m_2 is the mass of crucible with the powdered raw materials, g; m_3 is the mass of the crucible containing the prepared biochar, g.

2.3. Experimental methods of sorption for SMX and Cu

Experiments were conducted in the laboratory of Gansu Province Wastewater Treatment Industry Technology Center. At 298K, twenty-five milliliters of a certain concentration of SMX or Cu(II) solution and a fixed mass of biochar (HBC300 or HBC600) were together added to a 50 mL Erlenmeyer flask for sorption kinetic experiments by the batch equilibrium experiment method, in which the sampling time was set from 0.1 to 24 h. The sorption isotherm experiments were divided into two groups. In the first group, the initial concentration of fixed SMX was 50 mg/L, and the concentration gradient of Cu(II) solution was 50-500 mg/L. In the second group, the initial concentration of the fixed Cu(II) solution was 200 mg/L, and the SMX concentration gradient was 10-100 mg/L. Then these Erlenmeyer flasks were placed in a constant temperature shaker and shaken at 150 rpm for 24 h. The suspension after shaking was filtered through a 0.45 μm

filter membrane for SMX and Cu analyses, where SMX was analyzed by High Performance Liquid Chromatography (HPLC) and Cu was determined by flame atomic absorption spectrometry.

2.4. Kinetics sorption models

Quasi-first-order and quasi-second-order kinetic models are used to fit kinetic data as shown in equations (3) and (4).

Quasi-first-order kinetic equation:

$$Q_t = Q_e\left(1-e^{-k_1 t}\right) \quad (3)$$

Quasi-second-order kinetic equation:

$$Q_t = \frac{Q_e^2 k_2 t}{1+Q_e k_2 t} \quad (4)$$

where Q_t is the amount of adsorbed substance at time t (h), mg/g; Q_e is the amount of adsorbed substance at equilibrium, mg/g; k_1 (h^{-1}) and k_2 [g/ (mg h)] are the adsorption rate constants of quasi-first-order and quasi-second-order kinetics, respectively.

2.5. Isotherm sorption models

Langmuir and Freundlich sorption equations are applied to fit the isothermal sorption data of the adsorbates as shown in equations (5) and (6).

Langmuir equation:

$$Q_e = \frac{Q_m K_L C_e}{1+K_L C_e} \quad (3)$$

Freundlich equation:

$$Q_e = K_F C_e^N \quad (6)$$

where Q_e is the amount of adsorbed substance at equilibrium, mg/g; C_e is the concentration of adsorbate at equilibrium, mg/L; Q_m is the saturated sorption amount of adsorbate on the biochar; K_L(L/mg), K_F ((L/g) ^{n}), and N are the constants of the equations.

2.6. Quantum chemical computational methods

In this study, the Vienna Ab mitio Simulation Package (VASP) was used for all density functional theory (DFT) calculations, and a generalized gradient approximation was applied to the Perdew-Burke-Ernzerhof (PBE) functional equation. The projected augmented wave potentials were used to describe the ion nuclei with a plane-wave basis set with a set-energy cut-off of 400 eV, the van der Waals interactions were geometrically optimized using the DFT-D3 empirical corrections All crystal structures were optimized with an energy convergence threshold of 1.0×10^{-5} eV for and force convergence threshold of 0.03 eV/Å. To avoid interaction between two adjacent surfaces, the vacuum spacing was set as 20.0 Å. and the sorption energies at each point are calculated according to equations (7).

$$E_{ads} = E_{tot}(\text{biochar+pollutant}) - E_{suf}(\text{biochar}) - E_{tot}(\text{pollutant}) \quad (7)$$

where E_{ads} is the sorption energy of the system, E_{tot} (biochar + pollutant) is the total energy of the pollutant sorption system of the biochar, E_{suf} (biochar) is the total energy of the point of the biochar surface, and E_{tot} (pollutant) is the energy of the pollutant at a single point.

3. Results and discussion

3.1. Characterization of biochar

Table 1 presents the physicochemical properties of biochar that has been synthesized at various temperatures. With increasing pyrolysis temperatures, the yield of biochar decreases from 18.12% of BC300 to 12.68% of BC600. This is mainly due to the original chemical bonds and biomass interior materials, such as cellulose, hemicellulose, and lignin, being destroyed in the pyrolysis process, generating volatile substances to escape and eventually causing the loss of biochar mass (Schmidt *et al.*2023). The ash content of the biochar has a positive correlation with the rise in temperature. However, compared with BC300 and BC600, the ash content of HBC300 and HBC600 is greatly reduced. This is attributed to the reaction between the carbonates and other substances in the ash and H^+ during the acid washing process. The pH values of HBC300 and HBC600 exhibit a smaller magnitude when compared to BC300 and BC600, owing to the alkaline ions in the biochar react with H^+ in the acid wash solution. The presence of weak metal salts (carbonates) in the ash of biochar is an important reason for the alkalinity of biochar (Yang *et al.*2022a). The C content increases from 57.71% (BC300) to 63.42% (BC600), indicating that the pyrolysis process of biomass is a carbon-rich process. The contents of O and H decrease with the increase in pyrolysis temperature, proving that deoxygenation and dehydrogenation occur in the pyrolysis of biomass (Mutsengerere *et al.*2019). H/C is widely used to evaluate the aromatization degree of biochar. The smaller the H/C, the higher the aromaticity and the stronger the stability of biochar (Calvelo Pereira *et al.*2011; Grutzmacher *et al.*2018; Shen *et al.*2023b). (N+O)/C is the polarity value of biochar. The polarity increases with the rise of (N+O)/C. Therefore, as the pyrolysis temperature increases, the aromaticity of the biochar increases, but the polarity decreases.

Table 1. Primary physicochemical parameters and elementary compositions of biochar

Samples	pH	Ash (%)	Element content (%)					Element ratio	
			C	H	N	O	S	(N+O)/C	H/C
BC300	9.64	16.9	57.71	2.85	1.01	21.27	0.26	0.39	0.05
BC600	10.6	23.4	63.42	1.24	1.13	10.45	0.36	0.18	0.02
HBC300	3.68	6.70	69.64	3.38	1.47	18.43	0.38	0.28	0.05
HBC600	3.62	7.04	77.70	1.77	1.51	11.50	0.48	0.17	0.02

Compared to BC300 and HBC300, the specific surface area (S_{BET}) of BC600 and HBC600 increases significantly, by nearly 100 times, with increasing pyrolysis temperature (**Table 2**). This is probably due to the higher pyrolysis temperature, which cracks the biomass feedstock into volatiles that escape from the biochar and increase the pore structure of the biochar (Li *et al.*2021).

Table 2. Porosity and BET surface areas of biochar

Adsorbent	$^1S_{BET}$ (m^2/g)	$^2S_{t-plot}$ (m^2/g)	$^3V_{pore}$ (cm^3/g)	$^4V_{micro}$ (cm^3/g)	$^5A_{BET}$
BC300	3.82	6.96×10^{-1}	6.75×10^{-3}	1.80×10^{-4}	7.06
BC600	3.16×10^{2}	2.20×10^{2}	1.59×10^{-1}	9.31×10^{-2}	2.01
HBC300	4.19	8.84×10^{-1}	5.52×10^{-3}	1.76×10^{-4}	5.26
HBC600	4.05×10^{2}	2.81×10^{2}	2.04×10^{-1}	1.19×10^{-1}	2.02

[1]BET Specific surface area; [2]t-plot Micro area; [3]Single point total volume; [4]t-pLot micropore volume; [5]BET average pore size

After acid washing, it is shown that the micropore area (S_{t-plot}) of HBC300 and HBC600 exhibits an increase. This rise suggests that the pore structure of biochar is blocked due to the presence of ash when the biochar is not subjected to acid washing. Following the acid washing process, most of the ash is removed from the biochar surface, and the pore structure on the biochar surface is exposed (Deng *et al.*2023). When the pyrolysis temperature is 300 °C, the irregular lamellar structures of biochar remains relatively intact (**Figure 1(a) and (c)**). When the pyrolysis temperature reaches 600 °C, volatiles spill out of the pores due to further partitioning of the biomass to liberate large amounts of energy. As a result, a clearer pore structure can be observed (**Figure 1(b) and (d)**).

As the pyrolysis temperature increases, the pores in the biochar burst out, making the pores more disorderly distributed, which is beneficial for improving the adsorption capacity of biochar. Compared to the biochar before and after acid washing, the pore structures of HBC300 and HBC600 are obviously exposed, the surface structures are clearer, and no excessive other debris or impurities are present, which may be due to the ash and impurities in the biochar being washed away by the acid solution (**Figure 1(c) and (d)**).

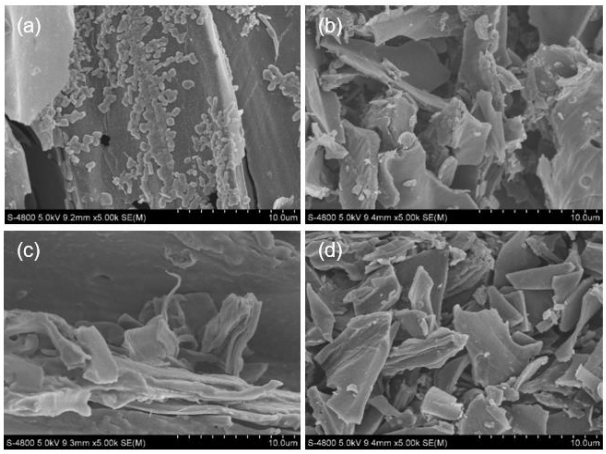

Figure 1. SEMs for BC300(a), BC600(b), HBC300(c), and HBC600(d)

The functional groups of biochar were characterized by FTIR. According to **Figure 2**, it can be seen that BC300, BC600, HBC300, and HBC600 have the same characteristic peaks. The absorption peak at 3421.46 cm^{-1} can be attributed to the stretching vibration of the hydroxyl group (-OH). The appearance of the hydroxyl group is due to a large amount of cellulose and hemicellulose in the biochar material is not destroyed at high temperatures. The absorbance peaks at 2993.73 cm^{-1} and 2826.94 cm^{-1} indicate the presence of the saturated alkanes -CH_2 and -CH_3. The peak at 2352.14 cm^{-1} may indicate the stretching vibration of C≡C or C=N. The peak at 1607.61 cm^{-1} is the C=C stretching vibration peak. The absorbance peaks between 1479.93 and 1375.32 cm^{-1} are mainly formed by the symmetric stretching of C=O in the carboxylate group COO-. The C-O stretching (1159.14 cm^{-1}) occurs due to the presence of hydrocarbons, indicating that hydroxyl and carboxyl groups may exist. The observed peaks at 978.79 cm^{-1} and 786.47 cm^{-1} can be attributed to the deformation of Si-O-Si. It can be seen from **Figure 2** that the positions of the characteristic absorption peaks of biochar prepared from the same material are roughly the same. However, there are variations in the values and widths of these absorption peaks, suggesting that biochars produced from the same source material possess similar functional groups, but the numbers are different (Anand *et al.*2023; Keiluweit *et al.*2010).

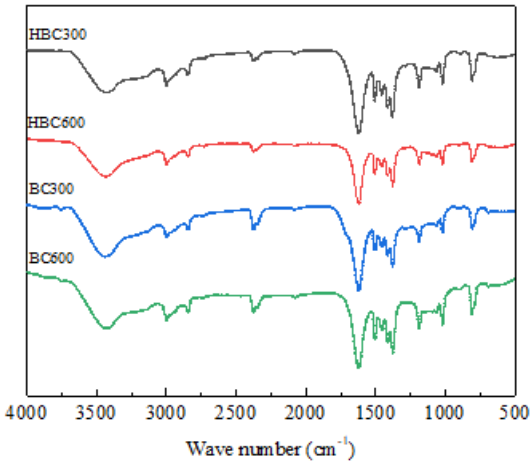

Figure 2. FTIR spectra for four types of biochar

3.2. Sorption kinetics

As shown in **Figure 3**, the amount of Cu/SMX adsorbed increases rapidly from 0 to 3 h, probably due to the presence of a large number of adsorption sites on the surface of the biochar and the high concentration of contaminants in the solution (Yan *et al.*2020). With increasing adsorption time, the adsorption rates slow down due to the limited number of adsorption sites on the biochar, and eventually reach adsorption equilibrium

at about 12 h. In the single system, the maximum adsorption capacities of Cu on HBC300 and HBC600 are 27.35 and 55.23 mg/g, respectively (**Figure 3(a)**). Similarly, it can be shown that the maximum adsorption capabilities for SMX are 6.14 and 21.61 mg/g on HBC300 and HBC600, respectively, as depicted in **Figure 3(b)**. Obviously, the adsorption capacities of biochar for Cu are higher than those for SMX. This may be due to the fact that there exists a large number of negative charges on biochar that can continue to interact with Cu (Wang and Liu 2017). Meanwhile, the adsorption capacities of HBC600 for SMX and Cu are higher than those of HBC300. This may be due to the higher the pyrolysis temperature, the greater the specific surface area of the biochar, and the stronger the adsorption for absorbates (Wang *et al.*2022).

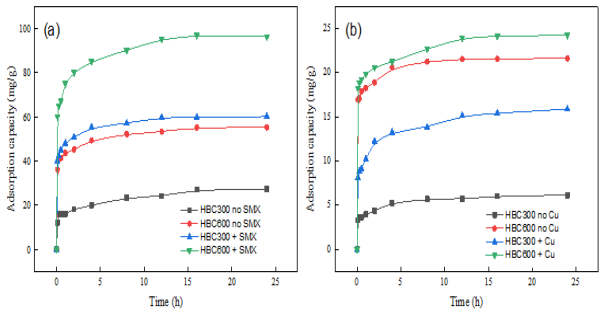

Figure 3. Effect of time on sorption of Cu(a) and SMX(b)

Compared with the single system, the adsorption capacity of HBC300 and HBC600 for SMX and Cu(II) in the mixed system increases to a certain extent. The maximum sorption of SMX and Cu(II) by HBC600 in the mixed system reached 24.22 mg/g and 96.23 mg/g at 24h, which was higher than the single sorption capacity of some modified biochar. For example, the maximum sorption of SMX was only 14.73 mg/g for chitosan-biochar (Son Tran *et al*. 2023), and the maximum sorption of Cu was only 38.6 mg/g for biochar loaded with MgAl-layered double hydroxide (Su *et al*. 2022). Therefore, during the adsorption process, the synergistic effect between SMX and Cu(II) has an important influence on the final adsorption capacity. The presence of Cu(II) can not only exchange the cation in biochar, but also form a complex with SMX that are easily adsorbed by the biochar. The complex has a strong affinity for biochar, resulting in enhanced adsorption of SMX and Cu(II) on the biochar (Xu *et al.* 2023). In addition, π-electron interaction is emphasized for chemicals with electron-donating. While the biochar adsorbs Cu(II), the SMX adsorbed on the biochar can also combine with Cu(II) to further increase the adsorption capacity of Cu(II).

In order to study the adsorption rate in mixed system, quasi-first-order and quasi-second-order kinetic equations were used to fit the kinetic data (**Table 3**). The equilibrium adsorption capacities, Q_e, of the two pollutants in mixed system are higher than those in the single system, but there is a certain increase in the difference in adsorption capacities due to the different adsorption orders of two different types of pollutants. The adsorption capacity of Cu increases greatly with the addition of SMX. The quasi-second-order rate constant, k_2, in the mixed adsorption system increases greatly on HBC600 (from 0.46 to 1.24 g/(mg·h)) and HBC300 (from 0.32 to 0.97 g/(mg h)). This may be due to, on the one hand, Cu(II) undergoes reactions, such as ion exchange and surface pore adsorption, on the surface of the biochar in the mixed system; on the other hand, Cu(II) complexes with SMX, forming the Cu(II)-SMX complex, which leads to a significant increase in the adsorption capacity (Yao *et al.*2020).

Table 3. Kinetic parameters of sorption of SMX and Cu(II) onto biochars

Pollutants	Biochar	quasi-first-order dynamics			quasi-second-order dynamics		
		Q_e (mg/g)	k_1 (h^{-1})	R^2	Q_e (mg/g)	k_2 (g/(mg·h))	R^2
SMX	HBC600 + Cu	18.07	0.50	0.8410	24.12	0.23	0.9715
	HBC600 no Cu	11.30	0.85	0.7496	19.60	0.13	0.9301
	HBC300 + Cu	12.34	0.02	0.8681	15.01	0.68	0.9017
	HBC300 no Cu	7.03	0.03	0.9177	6.29	0.48	0.9246
Cu (II)	HBC600 + SMX	70.12	0.42	0.8864	95.44	1.24	0.9821
	HBC600 no SMX	55.02	0.01	0.9118	60.34	0.46	0.9491
	HBC300 + SMX	48.70	0.51	0.9204	54.78	0.97	0.9120
	HBC300 no SMX	25.00	0.01	0.8573	27.01	0.32	0.9588

As shown in **Table 3**, the R^2 values of the quasi-first-order kinetic model are lower than those of the quasi-second-order kinetic model. Moreover, the theory adsorption amounts of the quasi-second-order kinetic model are closer to the actual values, indicating that the quasi-second-order kinetic model is more suitable for describing the adsorption process of SMX and Cu(II) on biochar. The whole adsorption process includes the composite reaction of surface adsorption and intra-particle diffusion adsorption. Therefore, the quasi-second-order kinetic model can reflect the kinetic mechanism of this adsorption more comprehensively (Fang *et al.* 2014; Ho 2006). In addition, the adsorption rate constants of the mixed system are higher than those of the single system, indicating that the mixed system favors the adsorption efficiencies of biochar for SMX and Cu(II).

3.3. Isothermal sorption

The adsorption isotherms of SMX and Cu are depicted in **Figure 4**, and the fitting parameters for SMX and Cu are summarized in **Table 4**. As shown in **Figure 4**, the amount of SMX and Cu(II) adsorbed by biochar increases with the equilibrium concentration. In the single system, due to the large number of anions on the surface of biochar, Cu(Ⅱ)

ions undergo an adsorption reaction with these anions through electrostatic attraction. At the same time, there are a large number of functional groups on the surface of biochar, which allow heavy metals to precipitate or complex with these functional groups. SMX molecules contain electron-poor parts (protonated amino groups), so they can act as electron acceptors. The aromatic structure of biochar makes it a powerful π electron donor, therefore functional groups have strong π-electron interactions with the aromatic structure. Compared with the single system, adsorption capacity in the mixed system increased significantly (**Figure 4(a)**). The maximum adsorption capacity of Cu on HBC300 increases from 18.74 mg/g in the single system to 159.80 mg/g in the mixed system. As for HBC600, the maximum adsorption capacity of Cu increased from 24.01 mg/g in the single system to 249.05 mg/g in the mixed system. Therefore, it is considered that Cu removal can be promoted when the SMX is present. It could be because when the porous in the biochar are filled in by single Cu adsorption, the sorption is difficult to continue. However, when SMX is added to the sorption system, -OH on the biochar could combine with SMX to produce intermediates that sequentially coordinate with Cu(Ⅱ). In the same way, the amount of SMX adsorbed increases significantly with the presence of Cu. This may be due to not only the pore adsorption and hydrogen bonding, but also that the adsorbed Cu(Ⅱ) on the biochar can act as a bridging bond for the adsorption of SMX. In addition, biochar also contains rich carboxyl groups (-COOH), phenolic hydroxyl groups (-OH), and other oxygen-containing functional groups that can form complexes with SMX and Cu(Ⅱ). Langmuir and Freundlich models were used to fit the isothermal data of SMX and Cu(Ⅱ) adsorbed by biochar (**Table 4**).

Table 4. Sorption isotherms parameters of SMX and Cu(Ⅱ) onto biochar

Pollutants	Biochar	Langmuir			Freundlich		
		Q_m (mg/g)	K_L (L/mg)	R^2	K_F ((L/g)^n)	*1/n*	R^2
SMX	HBC600 + Cu	35.07	0.50	0.8352	19.90	0.23	0.9706
	HBC600 no Cu	31.30	0.85	0.9310	19.60	0.13	0.9821
	HBC300 + Cu	25.34	0.02	0.9661	2.34	0.68	0.9785
	HBC300 no Cu	18.03	0.92	0.9247	1.59	0.48	0.9641
Cu(Ⅱ)	HBC600 + SMX	240.12	0.42	0.9203	2.36	1.24	0.9516
	HBC600 no SMX	25.02	0.01	0.8619	1.12	0.46	0.9742
	HBC300 + SMX	164.70	0.51	0.9476	2.04	0.97	0.9599
	HBC300 no SMX	24.76	0.01	0.8858	1.23	0.32	0.9651

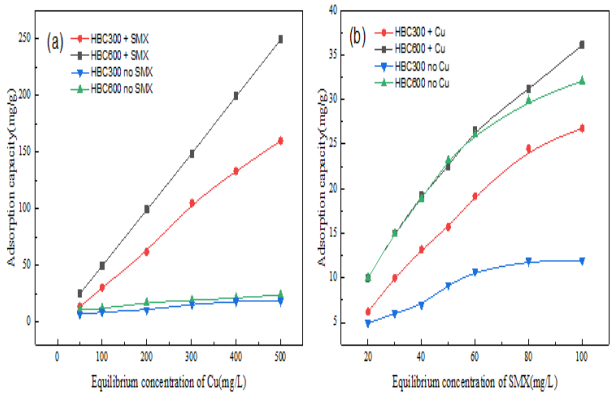

Figure 4. Sorption isotherms of Cu(II)(a) and SMX(b) on biochar

When the adsorption capacity of the adsorbent is strong, it can better conform to the Freundlich adsorption isotherm and deviate from the Langmuir isotherm. As the R^2 values of the Freundlich model range from 0.95 to 0.98 (**Table 4**), the Freundlich model fits better than the Langmuir model, indicating that the sorption of SMX and Cu on biochar is heterogeneous multilayer adsorption, including valence forces and van der Waals forces(Stromer *et al.*2018). Judging from the parameters of the two sets of models, the adsorption capacity of the mixture system is enhanced. Therefore, it can be inferred that co-adsorption has a certain promotion effect on the removal of pollutants compared with single adsorption.

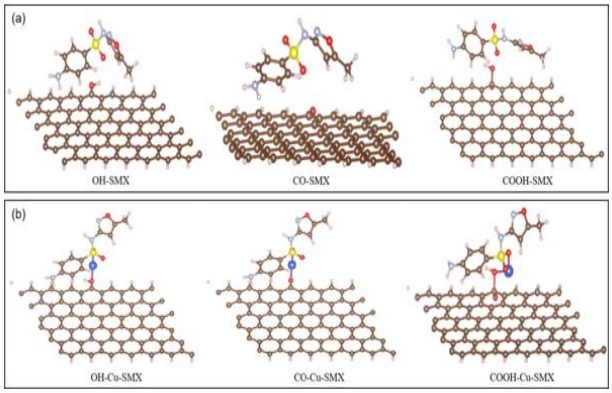

Figure 5. Optimized configurations of sorption models for biochar in single(a) and mixed(b) systems

3.4. Quantum chemical calculation results

From the analysis of the kinetic and isothermal sorption, it can be seen that there may be OH-SMX bond, CO-SMX bond and COOH-SMX bond between biochar and SMX. Three kinds of O containing functional groups on biochar including -OH, -CO and -COOH were considered as adsorption sites for SMX and SMX-Cu complex. As shown in **Table 5**, Compared with -O and -COOH, the sorption energy of SMX on -OH group of biochar is more negative, suggesting that -OH group was the main sites for absorbing SMX. In addition, the sorption energies of OH-Cu-SMX (-2.88 eV), CO-Cu-SMX (-3.12 eV), and COOH-Cu-SMX (-3.93 eV) formed by the simultaneous sorption of

SMX and Cu on the biochars were smaller than those of OH-SMX (-1.63 eV), CO-SMX (-1.58 eV), and COOH -SMX bonds (-0.49 eV), indicating that the sorption of pollutants by biochar is more favorable when two pollutants are co-existing. Moreover, for all -OH, -CO and -COOH biochar configurations, the bond between Cu-SMX with biochar was clearly found (**Figure 5**). The above results verified that Cu could act as bridge to enhance the adsorption of SMX on biochar.

Table 5. Total system energy and sorption energy for different binding units on biochar

	Calculation unit	Total system energy (eV)	sorption energy (eV)
pre-sorption	-OH	-829.51	-
	-CO	-826.12	-
	-COOH	-834.32	-
	-SMX	-177.46	-
	-Cu-SMX	-177.80	-
post-sorption	-OH-SMX	-1008.60	-1.63218923
	-CO-SMX	-1005.17	-1.58166821
	-COOH-SMX	-1012.27	-0.48921977
	-OH-Cu-SMX	-1010.19	-2.88216571
	-CO-Cu-SMX	-1007.04	-3.11984307
	-COOH-Cu-SMX	-1016.05	-3.93211981

4. Conclusions

This study examines the interaction between SMX and Cu on biochar. The results indicated that in the mixed system, SMX and Cu have a synergistic effect on each other in the adsorption process of maize straw biochar. When sorption equilibrium is reached, the optimum adsorption capacity of HBC600 for Cu in the mixed system (96.23 mg/g) is much higher than that of the single system (55.23 mg/g) in the mixed system. Similarly, the optimum adsorption capacity of HBC600 for SMX is 24.22 mg/g in the mixed system, which is higher than that of the single system (21.61 mg/g). Compared to the single system, the equilibrium adsorption capacities of HBC300 and HBC600 for SMX and Cu(Ⅱ) in the mixed system exhibited a notable increase, accompanied by a reduction in the time required to attain adsorption equilibrium. This trend is consistent with the quasi-second-order kinetic equation, indicating that the adsorbent has a strong sorption capacity in the mixed system. In addition, the adsorption process was consistent with the Freundlich isotherm model, indicating the multilayer heterogeneous sorption behavior of biochar in the mixed system. According to the quantum chemical calculation results, OH-Cu-SMX, CO-Cu-SMX and COOH-Cu-SMX bonds were formed on the biochar in the mixed system, and the sorption energies were greater than those in the single system, indicating that it is more favorable for the sorption of the two pollutants on the biochar in the mixed system.

Acknowledgements

All authors contributed to the study conception and design. We thank Yin Zhang, Yuanhu Gao, Jing Li, and Lin Liu for material preparation, data collection, and analysis, Yixiang Bao for assistance with computational analysis of quantum chemistry, Jiawen He for writing the manuscript, and Jinkui Zhong for methodological, writing-review, and editorial guidance. All authors read and approved the final manuscript.

Funding

This work was supported by National Natural Science Foundation of China (22366025), Plan Project of Science and Technology of Gansu Province (20JR2RA002), Project of Innovation and Entrepreneurship for Undergraduates in Lanzhou Jiaotong University (DC2410732CX0011)

Declarations statement

Ethical approval

Not applicable.

Consent to participate

Not applicable.

Consent to publish

Not applicable.

Competing interests

The authors declare no competing interests.

References

Alfaro Soto M.A., Lenhard R., Chang H.K. and andvan Genuchten M.T. (2019), Determination of specific LNAPL volumes in soils having a multimodal pore-size distribution, *Journal of Environmental Management*, **237**, 576–584.

Anand A., Gautam S. andRam L.C. (2023), Feedstock and pyrolysis conditions affect suitability of biochar for various sustainable energy and environmental applications, *Journal of Analytical and Applied Pyrolysis*, **170**, 105881.

Calvelo Pereira R., Kaal J., Camps Arbestain M., Pardo Lorenzo R., Aitkenhead W., Hedley M., Macías F., Hindmarsh J. and Maciá-Agulló J.A. (2011), Contribution to characterisation of biochar to estimate the labile fraction of carbon, *Organic Geochemistry*, **42**, 1331–1342.

Cuprys A., Pulicharla R., Lecka J., Brar S.K., Drogui P. and Surampalli R.Y. (2018). Ciprofloxacin-metal complexes-stability and toxicity tests in the presence of humic substances, *Chemosphere*, **202**, 549–559.

Deng L., Zhao Y., Sun S., Feng D. and Zhang W. (2023), Thermochemical method for controlling pore structure to enhance hydrogen storage capacity of biochar, *International Journal of Hydrogen Energy*, **48**, 21799–21813.

Deng R., Huang D., Zeng G., Wan J., Xue W., Wen X., Liu X., Chen S., Li J., Liu C. and Zhang Q. (2019), Decontamination of lead and tetracycline from aqueous solution by a promising carbonaceous nanocomposite: Interaction and mechanisms insight, *Bioresource Technology*, **283**, 277–285.

Fang C., Zhang T., Li P., Jiang R.F. and Wang Y.C. (2014), Application of Magnesium Modified Corn Biochar for Phosphorus Removal and Recovery from Swine Wastewater, *International Journal of Environmental Research and Public Health*, **11**, 9217–9237.

Gao S., Zhao Z., Xu Y., Tian J., Qi H., Lin W. and Cui F. (2014), Oxidation of sulfamethoxazole (SMX) by chlorine, ozone and permanganate-A comparative study, *Journal of Hazardous Materials*, **274**, 258–269.

Grutzmacher P., Puga A.P., Bibar M.P.S., Coscione A.R., Packer A.P. and de Andrade C.A. (2018), Carbon stability and mitigation of fertilizer induced N_2O emissions in soil amended with biochar, *Science of The Total Environment*, **625**, 1459–1466.

Guo M., Song W. and Tian J. (2020), Biochar-Facilitated Soil Remediation: Mechanisms and Efficacy Variations, *Frontiers in Environmental Science*, **8**, 521512.

Han Z., Zhang Y., An W., Lu J., Hu J. and Yang M. (2020), Antibiotic resistomes in drinking water sources across a large geographical scale: Multiple drivers and co-occurrence with opportunistic bacterial pathogens, *Water Research*, **183**, 116088.

Ho Y.S. (2006), Review of second-order models for adsorption systems, *Journal of Hazardous Materials*, **136**, 681–689.

Hu T., Zhao S., Huang Y., Chen Z., Zhang X., Wei C., Zeng S. and Liu L. (2023), Potential removals of tetracycline and sulfamethoxazole by iron-loaded sludge biochar, *Journal of Water Process Engineering*, **54**, 103962.

Huang B., Liu Y., Li B., Liu S., Zeng G., Zeng Z., Wang X., Ning Q., Zheng B. and Yang C. (2017), Effect of Cu (II) ions on the enhancement of tetracycline adsorption by Fe_3O_4@SiO_2-Chitosan/graphene oxide nanocomposite, *Carbohydrate Polymers*, **157**, 576–585.

Keiluweit M., Nico P.S., Johnson M.G. and Kleber M. (2010), Dynamic Molecular Structure of Plant Biomass-Derived Black Carbon (Biochar), *Environmental Science & Technology*, **44**, 1247–1253.

Khurana P., Pulicharla R. and Kaur Brar S. (2021), Antibiotic-metal complexes in wastewaters: fate and treatment trajectory, *Environment International*, **157**, 106863.

Kwak J.H., Islam M.S., Wang S., Messele S.A., Naeth M.A., El Din M.G. and Chang S.X. (2019), Biochar properties and lead(II) adsorption capacity depend on feedstock type, pyrolysis temperature, and steam activation, *Chemosphere*, **231**, 393–404.

Li B., Xie X., Zhang L., Lin D., Wang S., Wang S., Xu H., Wang J., Huang Y., Zhang S. and Liu D. (2021), Coke formation during rapid quenching of volatile vapors from fast pyrolysis of cellulose, *Fuel*, **306**, 121658.

Li S., Hu S., Jiang W., Liu Y., Zhou Y., Liu Y. and Mo L. (2018), Hierarchical architectures of bismuth molybdate nanosheets onto nickel titanate nanofibers: Facile synthesis and efficient photocatalytic removal of tetracycline hydrochloride, *Journal of Colloid and Interface Science*, **521**, 42–49.

Li Y., Wu M., Wu J., Wang Y., Zheng Z. and Jiang Z. (2022), Mechanistic insight and rapid co-adsorption of nitrogen pollution from micro-polluted water over MgAl-layered double hydroxide composite based on zeolite, *Separation and Purification Technology*, **297**, 121484.

Liu L., Si L., Yang J., Peng L., Qiao S., Sun Y. and Guo C. (2023), Biodegradation and process optimization of phenol and formaldehyde by Aspergillus nomius SGFA1, *International Biodeterioration & Biodegradation*, **182**, 105630.

Liu X., Shao Y., Dong Y., Dong M., Xu Z., Hu X. and Liu A. (2021), Response of ammonia-oxidizing archaea and bacteria to sulfadiazine and copper and their interaction in black soils, *Environmental Science and Pollution Research*, **28**, 11357–11368.

Long L.L., Bai C.W., Zhang S.R., Deng S.H., Zhang Y.Z., He J.S., Wu J., Chen C. and Yang G. (2021), Staged and efficient removal of tetracycline and Cu^{2+} combined pollution: A designed double-chamber electrochemistry system using 3D rGO, *Journal of Cleaner Production*, **305**, 127101.

Mutsengerere S., Chihobo C.H., Musademba D. and Nhapi I. (2019), A review of operating parameters affecting bio-oil yield in microwave pyrolysis of lignocellulosic biomass, *Renewable and Sustainable Energy Reviews*, **104**, 328–336.

Pathy A., Pokharel P., Chen X., Balasubramanian P. and Chang S.X. (2023), Activation methods increase biochar's potential for heavy-metal adsorption and environmental remediation: A global meta-analysis, *Science of The Total Environment*, **865**, 161252.

Qiu L.Q., Zhang L., Tang K., Chen G., Kumar Khanal S. and Lu H. (2019), Removal of sulfamethoxazole (SMX) in sulfate-reducing flocculent and granular sludge systems, *Bioresource Technology*, **288**, 121592.

Schmidt M.P., Ashworth D.J., Celis N. and Ibekwe A.M. (2023), Optimizing date palm leaf and pistachio shell biochar properties for antibiotic adsorption by varying pyrolysis temperature, *Bioresource Technology Reports*, **21**, 101325.

Sha J., Li L., An Z., He M., Yu H., Wang Y., Gao B. and Xu S. (2022), Diametrically opposite effect of Cu^{2+} on sulfamerazine and ciprofloxacin adsorption-photodegradation in g-C_3N_4/visible light system: behavior and mechanism study, *Chemical Engineering Journal*, **428**, 131065.

Shan J., Ji R., Yu Y., Xie Z. and Yan X. (2015), Biochar, activated carbon and carbon nanotubes have different effects on fate of ^{14}C-catechol and microbial community in soil, *Scientific Reports*, **5**, 16000.

Shen C., He M., Zhang J., Liu J., Su J. and Dai J. (2023a), Effects of the coexistence of antibiotics and heavy metals on the fate of antibiotic resistance genes in chicken manure and surrounding soils, *Ecotoxicology and Environmental Safety*, **263**, 115367.

Shen J., Wu Y., Lan G., Xia Y., Yan B., Li Y., Zhang Y., Yu Y., Fu C., Xu A., Zhou J., Zhu A. and Chen D. (2023b), Effect of co-pyrolysis of sewage sludge with different plastics on the nitrogen, sulfur, and chlorine releasing characteristics and the heavy metals ecological risk of biochar, *Journal of Environmental Chemical Engineering*, **11**, 110406.

Shu Y., Li D., Xie T., Zhao K., Zhou L. and Li F. (2024), Antibiotics-heavy metals combined pollution in agricultural soils:

Sources, fate, risks, and countermeasures, *Green Energy & Environment*.

Son Tran V., Hao Ngo H., Guo W., Ha Nguyen T., Mai Ly Luong T., Huan Nguyen X., Lan Anh Phan T., Trong Le V., Phuong Nguyen M. and Khai Nguyen M. (2023), New chitosan-biochar composite derived from agricultural waste for removing sulfamethoxazole antibiotics in water, *Bioresource Technology*, **385**, 129384.

Stromer B.S., Woodbury B. and Williams C.F. (2018), Tylosin sorption to diatomaceous earth described by Langmuir isotherm and Freundlich isotherm models, *Chemosphere*, **193**, 912–920.

Su X., Chen Y., Li Y., Li J., Song W., Li X. and Yan L. (2022), Enhanced adsorption of aqueous Pb(II) and Cu(II) by biochar loaded with layered double hydroxide: Crucial role of mineral precipitation, *Journal of Molecular Liquids*, **357**, 119083.

Tong F., Zhao Y., Gu X., Gu C. and Lee C.C.C. (2015), Joint toxicity of tetracycline with copper(II) and cadmium(II) to Vibrio fischeri: effect of complexation reaction, *Ecotoxicology*, **24**, 346–355.

Truong Q.M., Ho P.N.T., Nguyen T.B., Chen W.H., Bui X.T., Kumar Patel A., Rani Singhania R., Chen C.W. and Dong C.D. (2022), Magnetic biochar derived from macroalgal Sargassum hemiphyllum for highly efficient adsorption of Cu(II): Influencing factors and reusability, *Bioresource Technology*, **361**, 127732.

Wang W., Kang R., Yin Y., Tu S. and Ye L. (2022), Two-step pyrolysis biochar derived from agro-waste for antibiotics removal: Mechanisms and stability, *Chemosphere*, **292**, 133454.

Wang Y. and Liu R. (2017), Comparison of characteristics of twenty-one types of biochar and their ability to remove multi-heavy metals and methylene blue in solution, *Fuel Processing Technology*, **160**, 55–63.

Wang Y., Wang X., Li J., Li Y., Xia S., Zhao J., Minale T.M. and Gu Z. (2019), Coadsorption of tetracycline and copper(II) onto struvite loaded zeolite–An environmentally friendly product recovered from swine biogas slurry, *Chemical Engineering Journal*, **371**, 366–377.

Xu Z., Huang W., Wang S., Song H., Xu J., Mailhot G., Tong Z., Zhang H. and Li Z. (2023), Co-adsorption characteristics of antibiotics with different functional groups and cadmium combined contamination on activated carbon, *Journal of Environmental Chemical Engineering*, **11**, 110070.

Yan L., Liu Y., Zhang Y., Liu S., Wang C., Chen W., Liu C., Chen Z. and Zhang Y. (2020), $ZnCl_2$ modified biochar derived from aerobic granular sludge for developed microporosity and enhanced adsorption to tetracycline, *Bioresource Technology*, **297**, 122381.

Yan S., Subramanian S.B., Tyagi R.D., Surampalli Rao Y. and Zhang Tian C. (2010), Emerging Contaminants of Environmental Concern: Source, Transport, Fate, and Treatment, *Practice Periodical of Hazardous, Toxic, and Radioactive Waste Management*, **14**, 2–20.

Yang S., Zhang L. and Duan F. (2022a), Effects of acid pickling and nitrogen doping on the biochar-NO reaction performance of different biochars under high O2 conditions, *Journal of the Energy Institute*, **103**, 128–137.

Yang Y., Luo X., Zhang J., Ma X., Sun P. and Zhao L. (2022b), Sewage sludge-coconut fiber co-pyrolysis biochar: Mechanisms underlying synergistic heavy metal stabilization and ciprofloxacin adsorption, *Journal of Cleaner Production*, **375**, 134149.

Yao N., Li C., Yu J., Xu Q., Wei S., Tian Z., Yang Z., Yang W. and Shen J. (2020), Insight into adsorption of combined antibiotic-heavy metal contaminants on graphene oxide in water, *Separation and Purification Technology*, **236**, 116278.

Yao Y., Gao B., Chen H., Jiang L., Inyang M., Zimmerman A.R., Cao X., Yang L., Xue Y. and Li H. (2012), Adsorption of sulfamethoxazole on biochar and its impact on reclaimed water irrigation, *Journal of Hazardous Materials*, **209-210**, 408–413.

You X., Li H., Pan B., You M. and Sun W. (2022), Interactions between antibiotics and heavy metals determine their combined toxicity to Synechocystis sp, *Journal of Hazardous Materials*, **424**, 127707.

Younes H.A., Mahmoud H.M., Abdelrahman M.M. and Nassar H.F. (2019), Seasonal occurrence, removal efficiency and associated ecological risk assessment of three antibiotics in a municipal wastewater treatment plant in Egypt, *Environmental Nanotechnology, Monitoring & Management*, **12**, 100239.

Yuan L., Yan M., Huang Z., He K., Zeng G., Chen A., Hu L., Li H., Peng M., Huang T. and Chen G. (2019), Influences of pH and metal ions on the interactions of oxytetracycline onto nano-hydroxyapatite and their co-adsorption behavior in aqueous solution, *Journal of Colloid and Interface Science*, **541**, 101–113.

Zhao R., Ding W., Sun M., Yang L., Liu B., Zheng H. and Li H. (2022), Insight into the co-removal of Cu(II) and ciprofloxacin by calcite-biochar composite: Enhancement and competition, *Separation and Purification Technology*, **287**, 120487.